Measurement 82 (2016) 94–104

Contents lists available at ScienceDirect

Measurement

journal homepage: www.elsevier.com/locate/measurement

Comprehensive study of Howland circuit with non-ideal components to design high performance current pumps

Amin Mahnam *, Hassan Yazdanian, Mohsen Mosayebi Samani

Biomedical Engineering Department, School of Engineering, University of Isfahan, Isfahan, Iran

ARTICLE INFO

Article history:
Received 8 May 2015
Received in revised form 13 November 2015
Accepted 28 December 2015
Available online 2 January 2016

Keywords:
Current source
Howland circuit
Impedance measurement
Output impedance

ABSTRACT

Howland circuit is a popular high performance, voltage-controlled current pump, which can both sink and source precise amounts of current and provide high output impedance as well as high frequency bandwidth. In this article, analytical expressions are derived for performance characteristics of non-ideal Howland Current Pump, and it is shown that the main characteristics can be adjusted using three independent parameters: resistors' scale, feedback ratio, and current sensing resistor's value. The derived expressions are evaluated by computer simulations, and then are used to design a current pump for an impedance cardiography system, as an example. Performance of the circuit is evaluated based on simulations and experimental tests, and then is compared with several previous designs in the literature. The relationships provide a unified framework for the analysis of different configurations of Howland current pump and can facilitate its design process for different applications with specific performance requirements.

1. Introduction

Electrical current pumps are used in various instruments including those for medical applications to deliver a controllable amount of current to the load (tissue) [1–4]. Two main applications are neural stimulators [1,5–9] and bio-impedance measurement systems. The latter includes electrical impedance tomography (EIT) systems [10–13], impedance cardiography (ICG) [14–16], and bio-impedance spectroscopy systems (BIS) [17,18]. In these applications, a highly stable, usually high frequency current is injected into the tissue to record accurate measurements of the impedance [2,10].

Different circuit topologies implementing current sources have been suggested to be used in these systems [13,19–27]. A common problem in the current pumps is that their performance, especially the output impedance, degrades significantly in high frequencies due to unintended capacitors in active elements. Howland circuit [28] is extensively used to design current pumps [11,12,29–32] due to its bidirectional output, ultra high output impedance as high as several mega ohms at the working frequency [11,30], stable output response over a wide frequency bandwidth as high as several mega Hertz [30,33], as well as the ability to generate arbitrary current waveforms. Some studies have investigated the characteristics and performance of Howland current pump (HCP) in its different configurations. The sensitivity to the tolerance of resistors has been studied for the standard, known also as "modified", configuration of HCP (Fig. 1) [34,35]. Pouliquen et al. [5] have studied the effect of input bias current, offset voltage, slew rate, and output swing of the op-amp on performance of "basic" HCP (See Section 3.1 for the definition). Hammod et al. [36] presented a noise analysis of basic and standard HCP circuits and demonstrated superior temperature stability of the standard configuration. Moreover, the output impedance and the stability at high

* Corresponding author.
E-mail address: mahnam@eng.ui.ac.ir (A. Mahnam).

http://dx.doi.org/10.1016/j.measurement.2015.12.044
0263-2241/

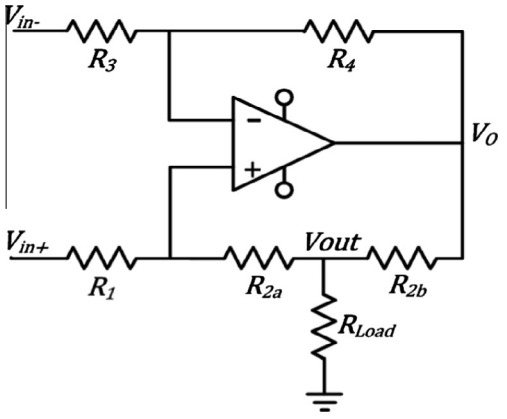

Fig. 1. Schematic of the standard form of Howland current pump.

frequencies have been compared for different configurations of HCP [32,37].

A Generalized Impedance Converter (GIC) can be added at the output of HCP to cancel the parasitic capacitances, hence improving the output impedance of the pump [38]. Wang et al. [39] have demonstrated that the GIC can only cancel the parasitic capacitances in a small limited frequency band, while it degrades the stability of the circuit, and makes the output current vary with the frequency.

Tucker et al. [30] determined the minimum op-amp requirements for a specified precision of HCP. They analyzed the noise and compliance of the circuit, and suggested effective compensation strategies to achieve stability without sacrificing high output impedance. However, their work was limited only to the standard form of the HCP. Liu et al. [31] have performed simulations and experiments to demonstrate the higher performance of a so called "differential" configuration of HCP in comparison to the standard configuration in terms of output impedance, SNR and compliance. These benefits are obtained by floating the load. This is not applicable in some applications when the load must be grounded for safety.

The analyses of HCP provided in previous studies have been limited to specific configurations of the circuit and/or specific characteristics as needed in that study. In this article, a comprehensive theoretical analysis of the HCP circuit is performed, and it is shown that many important characteristics of the HCP can be written with respect to three main parameters of the circuit: the scale of the resistors used, the feedback ratio, and the value of the current sensing resistor in the positive feedback path.

The role of these parameters in enhancing different characteristics of the HCP is discussed, and extended to different popular configurations of the HCP circuit in a unified framework in order to compare the performance of these circuits for different applications. A series of simulations are presented to demonstrate the accuracy and the importance of the derived equations. The equations are then used to design a high performance HCP for an impedance cardiography system, as an example, and the measured performance of its practical implementation is reported to further evaluate the applicability of the equations. Moreover, the performance of the designed HCP was compared to the designs proposed in the literature. The analyses provide a deep insight into different HCP circuits, and the effect of design parameters on their performance. This further helps to design an appropriate version of HCP with optimized performance for each specific application.

2. Analysis of the standard HCP circuit

2.1. Ideal standard Howland Current Pump

Fig. 1 demonstrates the schematic of the standard Howland current pump. The load current is obtained as:

$$I_{\text{out}} = \frac{1}{R_{2b}}\frac{R_4}{R_3}\left(\frac{R_{2a}+R_2\frac{R_3}{R_4}}{R_{2a}+R_1}V_{\text{in}+}-V_{\text{in}-}\right) + \frac{R_4R_1-R_2R_3}{R_3R_{2b}(R_1+R_{2a})}V_{\text{out}}. \quad (1)$$

where R_2 is the sum of R_{2a} and R_{2b}. If the following relationship is assumed,

$$\frac{R_2}{R_1}=\frac{R_4}{R_3} \quad (2)$$

then the load current becomes independent of its voltage and is proportional to the differential input voltage of the circuit:

$$\frac{I_{\text{out}}}{V_{\text{in}+}-V_{\text{in}-}}=\frac{1}{R_{2b}}\frac{R_4}{R_3}=\frac{1}{R_{2b}}\frac{1-\beta_{\text{fb}}}{\beta_{\text{fb}}} \quad (3)$$

where $\beta_{\text{fb}} = R_3/(R_3 + R_4)$; and the circuit becomes a voltage to current converter with differential inputs.

The compliance of the HCP is restricted by the output range of the op-amp, and can be calculated from

$$V_O = \left(1+\frac{R_{2b}}{R_1+R_2-R_{2b}}\right)(V_{\text{out}}+(R_{2a}\|R_{2b})I_{\text{out}}) - \frac{R_{2b}}{R_1+R_2-R_{2b}}V_{\text{in}-} \quad (4)$$

Assuming $V_{in-} = 0$, Eq. (4) yields:

$$V_{out}(\max)=\frac{(\beta_{fb}+\frac{R_{2a}}{R_1+R_2})}{\left(1+\frac{R_{2a}\|R_{2b}}{R_{Load}}\right)}V_O(max) \quad (5)$$

Eq. (5) gives the maximum output voltage of the HCP for a constant load and therefore it determines the upper limit of the output current. The equation shows that designing the HCP with larger feedback ratio β_{fb} would increase the compliance of the circuit. This is also true for smaller R_{2b} to R_{2a} ratio since the numerator in Eq. (5) increases and the denominator decreases ($R_{2a}\|R_{2b}$ decreases when R_{2b} get smaller than R_{2a}). A small enough R_{2b} (relative to R_{Load}) also leads to the independence of compliance from changes in the output current. Note that the compliance is improved for $V_{in-} > 0$.

The design process of the Howland current pump includes selection of feedback ratio β_{fb}, scale of the resistors used in the circuit (R_3, R_4, R_1 and R_{2a}) and R_{2b} value. However, in practice there are non-ideal characteristics of the components, which affect the performance of the circuit and should be considered in the design process.

These characteristics will be discussed in the following sections.

2.2. Influence of non-ideal parameters of HCP

2.2.1. Resistor Tolerance

Tolerance of the resistors can significantly degrade the ideal performance of the HCP. One can observe from (1) that violation from criterion (2) results in finite output resistance of the HCP as well as an imbalance between transfer functions of positive and negative inputs. For resistors with $T\%$ tolerance, the minimum output resistance can be calculated as:

$$R_{\text{out}} = \frac{(R_1 + R_2 - R_{2b}) \| R_{2b}}{1 - \beta_{fb}} \frac{(1-T)^2}{\pm 4T} \tag{6}$$

This implies that the output resistance of HCP significantly decreases with the tolerance of resistors. In addition, Eq. (6) implies that for a certain tolerance, the output resistance of the HCP can be improved by using large feedback ratio, large R_{2b}, and large resistors in the design.

The tolerance of the resistors also leads to an imbalance between positive and negative inputs of the HCP. The gain for negative input $V_{\text{in}-}$ stays the same, but that for the positive input changes. This can be viewed as a finite CMRR of the circuit:

$$\text{CMRR} = 1 + \frac{1}{2T}\left(1 + \frac{R_{2a}}{R_1}\right). \tag{7}$$

The CMRR is inversely proportional to the resistors tolerances. Small values of R_{2a} and large values of R_1 reduce the CMRR toward its lower limit of $1 + (1/2T)$. Therefore, smaller values of R_{2b} improve the CMRR and compliance of the HCP, while reduce its output resistance, considering a constant β_{fb}. On the other hand, for a constant R_{2b}/R_{2a} ratio, CMRR degrades for larger β_{fb}.

2.2.2. Offset voltage and Input bias current of the op-amp

Non-ideal behavior of the op-amp can also degrade the performance of the HCP. Considering the input offset voltage of the op-amp:

$$I_{\text{out}} = \frac{1-\beta_{\text{fb}}}{\beta_{\text{fb}} R_{2b}}(V_{\text{in}+} - V_{\text{in}-}) - \frac{1}{\beta_{\text{fb}} R_{2b}} V_{\text{off}} \tag{8}$$

which indicates that the output error is inversely proportional to the R_{2b} value and the feedback ratio.

Input bias current of the op-amp can also induce an error term in the output current:

$$I_{\text{out}} = \frac{1-\beta_{\text{fb}}}{\beta_{\text{fb}} R_{2b}}(V_{\text{in}+} - V_{\text{in}-}) - \frac{1}{R_{2b}}(R_4 I_{\text{b}-} - R_2 I_{\text{b}+}) \tag{9}$$

The above equation suggests the use of equal resistors for negative and positive feedback loops in the HCP circuit to minimize the output error due to input bias current of the op-amp. In this case, the error would be proportional to the input offset current, and can be kept small by using large R_{2b}.

2.2.3. Finite open loop gain

Considering the finite open loop gain of the op-amp, A, output current can be calculated from the following equation:

$$I_{\text{out}} = \frac{AR_2 + R_{2b}\frac{R_1+R_2}{R_1+R_{2a}}}{R_{2b}(AR_1 + R_1 + R_2)} V_{\text{in}+} - \frac{AR_4}{R_{2b}(AR_3 + R_3 + R_4)} V_{\text{in}-} - \frac{V_{Out}}{\left(1 + \frac{AR_3}{R_3+R_4}\right)(R_{2b} \| (R_1 + R_{2a}))}. \tag{10}$$

Obviously, the finite open loop gain of the op-amp results in finite output resistance and CMRR of the HCP.

$$R_{\text{out}} = (R_{2b} \| (R_1 + R_2 - R_{2b}))(1 + A\beta_{\text{fb}}) \tag{11}$$

$$CMRR = 1 + 2AR_2\left(\frac{1}{R_{2b}} - \frac{1}{R_1 + R_2}\right) = 1 + 2A\left(\beta_{\text{fb}} + \frac{R_{2a}}{R_{2b}}\right) \tag{12}$$

Eq. (12) states that CMRR can be improved by larger β_{fb} and smaller R_{2b} to R_{2a} ratio. Note that small R_{2b} results in small output resistance of the circuit (Eq. (11)). However, it is possible to use large R_{2b} while keeping the R_{2b} to R_{2a} ratio small. In this way, appropriate R_{out} and CMRR are preserved. On the other hand, Eq. (10) implies that the ideal input–output relationship of the HCP is valid only for $A\beta_{\text{fb}} \gg 1$, since by assuming this, the coefficients of the input terms will become independent of A.

The effect of the resistors' tolerance and the finite open loop gain of the op-amp on the output resistance of the HCP are stated separately by using (6) and (11). However, simulations suggested that the simultaneous effect of these two factors is significant and may not be predicted by these equations separately. Therefore, Eq. (13) that states the effect of both factors on output resistance of the HCP, was derived:

$$R_{\text{out}} = \frac{((R_1 + R_{2a}) \| R_{2b})(1 + A\beta_{\text{fb}})}{1 + 4T(1 - \beta_{\text{fb}})\beta_{\text{fb}} A} \tag{13}$$

In this Equation, the same components as in (6) and (11) have appeared. However, the denominator has an additional multiplying factor of $\beta_{\text{fb}}A$ and is added to 1. According to (13), the output resistance of HCP can be improved by using large R_{2b}, large tightly matched resistors in the design, and a feedback ratio close to 1.

2.2.4. Limited bandwidth

To analyze the frequency behavior of the HCP, the op-amp can be considered as a simple one-pole system with cut-off frequency of ω_{b} and DC open loop gain of A_0 ($A(\omega) = A_0/(1 + j\omega/\omega_{\text{b}})$). Then, the output impedance of the HCP is calculated as:

$$Z_{\text{out}} = (R_{2b} \| (R_1 + R_{2a}))(1 + A_0\beta_{\text{fb}}) \left(\frac{1 + j\frac{\omega}{\omega_{\text{b}}(1 + A_0\beta_{\text{fb}})}}{1 + j\frac{\omega}{\omega_{\text{b}}}}\right). \tag{14}$$

The equivalent output impedance model of the HCP is a capacitive–resistive network shown in Fig. 2. For frequencies much greater than the cut-off frequency of the op-amp, R_{p} the resistor in parallel with capacitor C_{p} can be neglected, and the output impedance tends toward R_{s}. It should be noted that in practice, the parasitic or stray

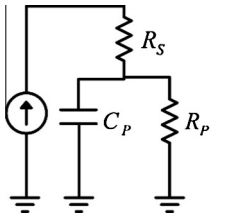

Fig. 2. Equivalent model of output impedance of the Howland current pump.

capacitances (due to switches in the output, or the capacitance between output tracks and wires and the ground) shunts some more current from the load, and effectively reduce the actual output impedance of the pump. This can be modeled as a parallel capacitance at the output of the HCP.

On the other hand, for frequencies much greater than ω_b, $A(\omega)$ can be approximated by $\omega_t/j\omega$ where ω_t is the unity-gain bandwidth of the op-amp. By substituting $A(\omega)$ in Eq. (10) with this approximation, the output current can be calculated as:

$$I_{out} = \frac{R_2}{R_1 R_{2b}\left(1 + j\frac{\omega}{\omega_t \beta_{fb}}\right)}\left(\left(1 + j\frac{\omega}{\omega_t \beta_{fb}}\frac{R_{2b}}{R_2\left(1 + \frac{R_{2a}}{R_1}\right)}\right)V_{in+} - V_{in-}\right). \quad (15)$$

The cut-off frequency of the HCP is therefore $\omega_t \beta_{fb}$. Note that the transfer function for the positive input contains a zero at a frequency higher than the cut-off frequency of the HCP. Despite this fact, the actual output current decreases with the frequency due to a reduction in the output resistance of the HCP.

2.2.5. Slew rate of the op-amp

As a current pump, the slew-rate of the circuit is defined here as the maximum rate of change of the output current. If $V_{in+} = 0$, the slew rate would be the worst, and it can be obtained from the following equation:

$$\frac{SR_{HCP}}{SR_{opamp}} = \frac{1}{R_{2b} + R_{Load}\left(1 + \frac{R_{2b}}{R_1 + R_{2a}}\right)}. \quad (16)$$

This suggests using large resistors in comparison to the load and also a small R_{2b} in order not to lose the slew rate of the op-amp.

2.2.6. Noise

The equivalent input noise of the HCP circuit can be calculated as follows [40]:

$$E_n = \sqrt{\left(4kT\frac{R_1 + R_3}{1 - \beta_{fb}} + i_n^2(R_1^2 + R_3^2) + e_n^2\frac{1}{(1 - \beta_{fb})^2}\right)BW_{eq}} \quad (17)$$

where $4kT\,(R_1 + R_3)/(1 - \beta_{fb})$ represents the thermal noise of the resistors, i_n is the input current noise density and e_n is the input voltage noise density of the op-amp, and BW_{eq} is the equivalent bandwidth of the circuit. Note that this equation is obtained by neglecting the $1/f$ noise for simplicity since it is only significant in very low frequencies. Eq. (17) demonstrates that the noise increases as a result of using large resistor values and greater feedback ratios.

2.3. Stability of HCP

Several methods have been suggested to improve the stability of the HCP. Steele and Green [34] have used a series RC 'snubber' network in parallel with the load to improve the stability. However, this technique works only for inductive loads, an uncommon condition in biomedical applications. The other technique is to use a capacitor in parallel with feedback resistor R_4 [10,41] which has the drawback of degraded output impedance at high frequencies, due to the violation of Eq. (2) [30]. However, the lead-lag compensator suggested by Tucker et al. [30] can significantly improve the phase margin, without degrading the output impedance. This can be done by adding a capacitor (C_c) and a resistor (R_c) in series between the inputs of the main op-amp in HCP. The compensator reduces the loop gain in high frequencies where the instability may occur, but not at the working frequency. With this compensator, the stable loop gain can be calculated as:

$$T_{stable} = \frac{1}{1 + 1/A(j\omega)\beta_{fb}}\left(\frac{1 + j\omega R_C C_c}{1 + j\omega(R_d + R_C)C_C}\right) \quad (18)$$

where R_d is the resistance seen by the compensating network:

$$R_d = (R_1 \| [R_{2a} + (R_{2b} + R_{Load})]) + (R_3 \| R_4) \quad (19)$$

To design the lead-lag compensator, a value for C_C an be selected, and then R_C should be adjusted to have the highest phase margin.

3. Analysis of other versions of HCP

3.1. Basic HCP

Basic Howland current pump, also referred to as "Simplified" Howland current pump, is a special case of HCP in which $R_{2a} = 0$, thus, $R_{2b} = R_2$, and therefore, its characteristics can be inferred from the previous equations. The gain for this configuration is calculated as $1/R_1$, which is the minimum gain of the HCP when R_{2b} changes from small values to $R_{2b} = R_2$. This may be a disadvantage of the basic HCP when high gain (more than hundreds of μA/V) and high input impedance are desired simultaneously.

The compliance of the HCP is also minimized in its basic configuration:

$$V_{out} = \beta_{fb} V_o + (1 - \beta_{fb})V_{in-} \quad (20)$$

The tolerance of the resistors has a significant effect on the output resistance of the basic HCP. Assuming $R_{2a} = 0$:

$$R_{out} = R_1\frac{(1 - T)^2}{\pm 4T} \quad (21)$$

While the use of larger R_1 increases the output resistance, it also directly affects the gain of the basic HCP. In addition, Eq. (7) shows that the CMRR is minimized in

the basic HCP (in comparison to the case when non-zero R_{2a} is used). However, output current error caused by the offset voltage and the input bias current of the op-amp is minimized in basic HCP, due to the large value of the R_{2b} (Eqs. (8) and (9)).

The finite open loop gain of the op-amp degrades the output resistance and the CMRR of the HCP (Eqs. (11) and (12)). However, large value of R_{2b} improves the R_{out} while reducing the CMRR of the HCP. Therefore, the basic HCP generally has better R_{out} but smaller CMRR in comparison to HCP with non-zero R_{2a} assuming that all the other parameters are constant.

In the basic HCP, the zero and pole of the transfer function for $V_{\text{in+}}$ cancel out each other (Eq. (15)). However, the load current is still affected by the frequency due to a decrease in its output resistance (Eq. (14)).

3.2. The bridge configuration

In this configuration, an extra op-amp is used as a unity-gain inverting amplifier to form a bridge as it is illustrated in Fig. 3.

This configuration almost doubles the compliance of the HCP for a floating load. The inverting amplifier can adjust the voltage of the other end of the load such that the desired current be able to pass the load, and therefore the differential voltage on the load can reach almost twice the value in the standard configuration. Since the inverting amplifier receives its input from the op-amp instead of the HCP output, the precision of the HCP is theoretically preserved. However, to ensure the best performance in practice, the value of R_5 must generally be high. Liu et al. [31] have compared the performance of a similar configuration with standard HCP and have shown that such a configuration significantly improves the output impedance. Besides, the slew rate of the HCP bridge configuration can be calculated as:

$$\frac{SR_{HCS}}{SR_{opamp}} = \frac{2 + \frac{R_{2b}}{R_1 + R_{2a}}}{R_{2b} + R_{Load}\left(1 + \frac{R_{2b}}{R_1 + R_{2a}}\right)} \tag{22}$$

which is more than twice as much as the slew rate of the standard HCP.

3.3. HCP with buffered feedback path

Fig. 4 shows another configuration of the HCP in which an extra op-amp is used to drive the positive feedback path

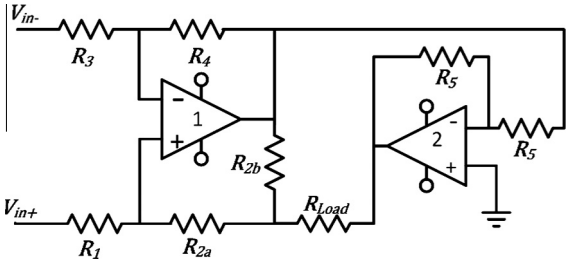

Fig. 3. Schematic of the HCP bridge configuration for a floating load.

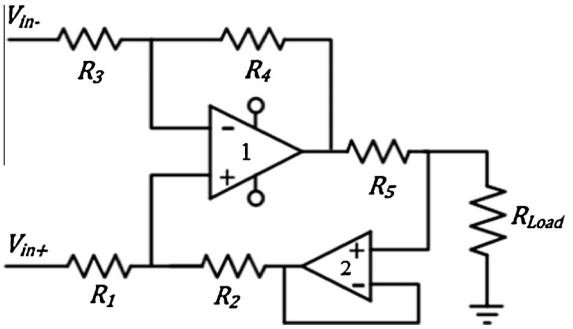

Fig. 4. HCP with buffered feedback path.

from the output node. Considering (2), the output current can be obtained as:

$$I_{\text{out}} = \frac{1}{R_5}\left(\frac{R_2}{R_1}V_{in+} - \frac{R_4}{R_3}V_{in-} + \left(\frac{R_4}{R_3} - \frac{R_2}{R_1}\right)V_{+}(Op_1)\right) = \frac{R_4}{R_3 R_5}(V_{\text{in+}} - V_{\text{in-}}). \tag{23}$$

The compliance of this configuration can be calculated from:

$$V_{\text{O\_max(Pump)}} = \frac{R_{Load}}{R_{Load} + R_5} V_{\text{O\_max(Op}_1\text{)}} \tag{24}$$

where Vo_max(Op1) is the maximum output voltage of op-amp 1.

The finite output resistance due to the resistors' tolerance is improved in this circuit in comparison with the standard configuration:

$$R_{\text{out}} \cong \frac{1}{\pm 4T}\frac{R_5}{1 - \beta_{\text{fb}}}. \tag{25}$$

The input offset voltage and input bias current of the second op-amp add extra error terms to the output current:

$$I_{\text{out}} = \frac{1 - \beta_{\text{fb}}}{\beta_{\text{fb}} R_5}(V_{\text{in+}} - V_{\text{in-}}) - \frac{1}{\beta_{\text{fb}} R_5}V_{off1} - \frac{1}{R_5}V_{off2} - \frac{1}{R_5}(R_4 I_{b1-} - R_2 I_{b1+}) - I_{b2}. \tag{26}$$

Considering the finite open loop gain of the op-amps, the output current can be calculated as:

$$I_{\text{out}} = \frac{A_1}{1 + A_1\beta_{\text{fb}}}\frac{1 - \beta_{\text{fb}}}{R_5}(V_{\text{in+}} - V_{\text{in-}}) - \frac{V_{\text{out}}}{R_5(1 + A_1\beta_{\text{fb}})} \tag{27}$$

where A_1 is the open loop gain of the forward path op-amp. This shows an increase in the output resistance compared to the standard HCP.

$$R_{out} = \frac{R_5(1 + A_1\beta_{\text{fb}})}{\left(\frac{A_1 A_2}{1 + A_2}\beta_{\text{fb}} - A_1\beta_{\text{fb}} - 1\right)} \tag{28}$$

where A_2 is open loop gain of the feedback path op-amp. However, the finite input impedance of this op-amp further reduce the output impedance of the pump.

Compared to the standard configuration, here the coefficients of positive and negative inputs of the pump are the

same; i.e. the pump is truly differential in inputs. Note that the finite open loop gain of the second op-amp has a negligible effect on the behavior of the circuit at low frequencies, but the effect may become significant in high frequencies. The frequency dependence of the op-amp gain results in a pole in the transfer function of the current pump:

$$I_{out} = \frac{A_1}{1 + A_1\beta_{fb}} \frac{1 - \beta_{fb}}{R_3} \frac{(V_{in+} - V_{in-})}{1 + j\frac{\omega}{\omega_b(1+A_1\beta_{fb})}}, \quad (29)$$

and a capacitive effect in the output impedance:

$$Z_{out} = R_5(1 + A_1\beta_{fb})\left(\frac{1 + j\frac{\omega}{\omega_b(1+A_1\beta_{fb})}}{1 + j\frac{\omega}{\omega_b}}\right). \quad (30)$$

The transfer function has no zero, and is symmetric for positive and negative inputs. The output impedance is also improved.

The slew rate is also improved in this configuration, and can be calculated as:

$$\frac{SR_{HCP}}{SR_{opamp}} = \frac{1}{R_5 + R_{Load}}. \quad (31)$$

4. Validation of the derived equations

To validate the accuracy of the derived equations, a series of simulations of the HCP performance were conducted with TINA design suit version 9.3 (DesignSoft company, Hungary). In these simulations, an ideal model of circuit components, except the one related to the specific equation under study was used. The performance of HCP with non-ideal models of components will be evaluated in the next section.

4.1. Simulation parameters

The resistor values for standard HCP, the bridge configuration, and HCP with buffered feedback path were selected as $R_1 = R_2 = R_3 = R_4 = 10\ k\Omega$, $R_{2a} = R_{2b} = 5\ k\Omega$, $R_5 = 5\ k\Omega$ and $R_{Load} = 50\ \Omega$. The resistor values for basic HCP were selected as $R_1 = R_3 = 5\ k\Omega$, $R_{2b} = R_4 = 10\ k\Omega$ and $R_{Load} = 50\ \Omega$ to have a current pump with the same gain and feedback ratio as the other configurations.

To evaluate the equations related to the non-ideal op-amp, specifications of the general purpose LM741 op-amp were used except otherwise stated, while for the rest of the equations the op-amp was considered ideal. LM741 was adopted for these simulations since its moderate specifications may better demonstrate the effect of non-ideal parameters of the op-amp on the HCP characteristics. The simulations were performed using two sine wave inputs of $1V_{p\text{-}p}$ each, with the frequency of 10 kHz, and 180° phase difference. The supply voltages of the op-amp were set to ± 15V. By these parameters, the amplitude of the output current is equal to 200 μA for all configurations. To evaluate the equations related to the tolerance of the resistors, one hundred simulations were executed with the resistor tolerance of 5%, and the worst result was reported (“worst-case” mode in TINA). The output impedance was obtained for zero inputs. The CMRR was also measured by performing two simulations with differential and common mode inputs. The finite output impedance and CMRR, resulted from finite open loop gain of the op-amp, were determined by considering an op-amp with gain 100 at 10 kHz. The slew rate of the HCP was evaluated in simulations by considering a square-wave voltage source of 0.5 V amplitude, 1 kHz, with 50% duty cycle for the negative input and by grounding the positive input. The op-amp slew rate was considered 0.5 V/μS. The bandwidth of the HCP was evaluated for LM741 op-amp with the unity gain bandwidth of 1 MHz.

4.2. Evaluation of general specifications

Table 1 compares the performance characteristics of different HCPs calculated from the equations and obtained in the simulations. The results are close together, and demonstrate the accuracy of the derived equations.

The compliance of Howland’s standard configuration is generally higher than the basic configuration, but less than buffered feedback configuration. As expected, the output impedance and CMRR (due to the tolerance of resistors) obtained from simulations are better than the worst-case values from the equations. The simulation results were converging to the values from equations as the number of simulation runs increased.

Table 1
Comparison of performance characteristics of Howland current pump due to non-ideal components based on the provided equations and performed simulations.

Configuration	Equation	Theory	Simulation
Compliance (V) (Vcc = ± 15 V)			
Standard	4	10.73	10.37
Basic	20	4.67	4.59
Bridge		≈2 × Standard	24.15
Buffered fdbk	24	14	13.93
Output Impedance (kΩ) (Resistor tolerance 5%)			
Standard	6	33.84	34.41
Basic	21	22.56	23.69
Buffered fdbk	25	50	55.13
CMRR (Resistor tolerance 5%)			
Standard	7	16	14.26
Offset of output current (μA) (V_{off} = 5 mV)			
Standard	8	2	1.78
Buffered fdbk	26	3	2.67
Offset of output current (μA) (I_{b-} = 500 nA, I_{b+} = 300n A)			
Standard	9	0.4	0.4
Buffered fdbk	27	0.6	0.6
Output Impedance (kΩ) (op-amp gain of 100 at 10 kHz)			
Standard	11	187.5	187.51
Buffered fdbk	28	175.85	166
CMRR (op-amp gain of 100 at 10 kHz)			
Standard	12	301	287.54
Slew Rate (A/s) ($SR_{op\text{-}amp}$ = 0.5 V/μs)			
Standard	16	98.68	98.41
Bridge	22	230.263	228
Buffered fdbk	31	99	98.96
Noise ($nV/Hz^{1/2}$) (e_n = 25 $nV/Hz^{1/2}$, i_n = 2 $pA/Hz^{1/2}$)			
Standard	17	62.89	69

4.3. Frequency response

Cut off frequencies of the standard and buffered feedback configurations were obtained 566 and 514 kHz respectively from simulations. These are close to the value of 500 kHz obtained from Eqs. (15) and (27) for these configurations. Moreover, Eq. (15) gives the value of 1.5 MHz for the zero of the transfer function in the standard configuration, while 1.26 MHz was obtained from simulations.

4.4. The effect of open loop gain on output impedance

Fig. 5 shows the output impedance vs. frequency for different configurations of HCP when linear LM741 model was used as the op-amp. DC open loop gain and cut-off frequency of LM741 was considered 200,000 and 5 Hz, respectively. This resulted in a cut-off frequency of 10 Hz and a slope of 10 dB/Dec for the impedance. The output impedance is significantly higher for bridge configuration and is the lowest for basic configuration. Please note that R1 value was considered half in basic configuration compared to other configurations which is the reason for lower output impedance. The buffered feedback configuration has a slightly lower output impedance compared with the standard one, because of the finite input impedance of the feedback op-amp.

The simulation was repeated for standard configuration when an op-amp with 10 and 20 times greater DC open loop gain was used, and the results (two upper curves in Fig. 5) demonstrate that the output impedance is sensitive to the open loop gain.

4.5. The effect of resistors tolerance on output impedance

Fig. 6 demonstrates the output impedance of standard HCP vs. frequency, when resistors with a tolerance of 0%, 0.01%, 0.1% and 1% and a linear model of LM741 was used. It can be noticed that tolerance of the resistors severely degrades output impedance of circuit at low frequencies. However, sensitivity of the output impedance on the tolerance decreases at high frequencies, where the open loop gain of the op-amp decreases. From Eq. (13) it is noticed that the impact of T on R_{out} lowers when the term $T(1-\beta_{fb})\beta_{fb}A$ approaches 1. Then open loop gain will be the dominating factor degrading the output impedance. The converged value of the output impedance is $R_{2b}||(R_1+R_{2a})$ (here, 3.75 kΩ) as can be seen from Eq. (14) and in Fig. 2. The appropriate value for the output impedance depends on the application in which the HCP is used. Values up to several ten mega ohms are reported in the literature.

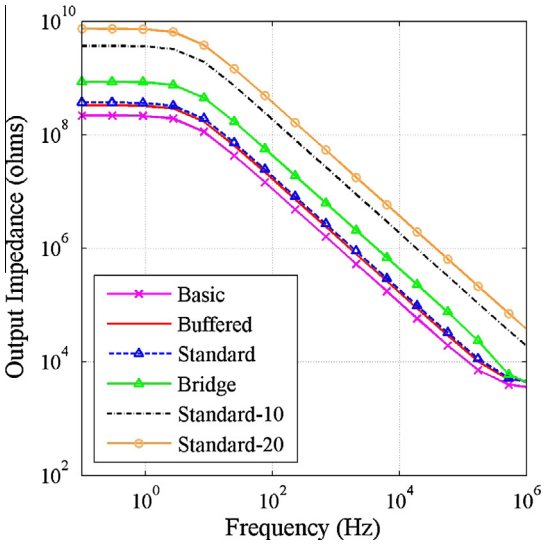

Fig. 5. Comparison of output impedance for different configurations of HCP considering the finite open loop gain and bandwidth of the op-amp (linear model of LM741 in 4 lower traces). The two upper traces are for when an op-amp identical to LM741 but with 10 and 20 times greater DC open loop gain was used.

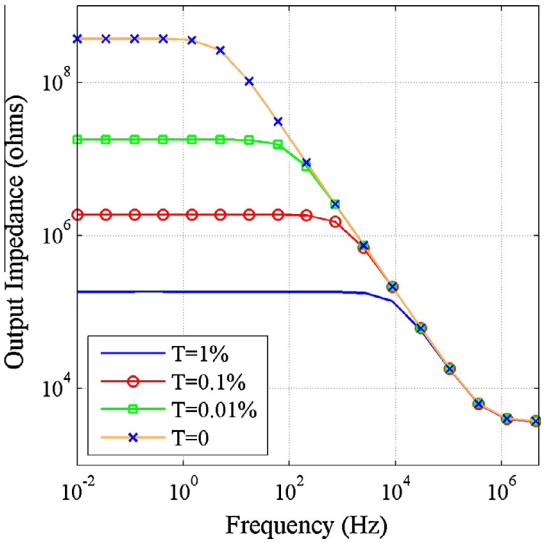

Fig. 6. Output impedance of standard HCP vs. frequency in 4 cases of 0%, 0.01%, 0.1% and 1% resistor tolerances.

5. Design of a current pump for ICG

Impedance cardiography (ICG) is a non-invasive technique of measuring the hemodynamics for monitoring the cardiac mechanical efficiency. ICG systems apply a high frequency (20–100 kHz) electrical current (1–5 mA) to the chest and measure the resulting voltage with the same or other pair of electrodes to calculate the thorax impedance. The applied current follows a path of the least resistance through the chest, which includes the blood filled aorta, and is therefore related to the hemodynamics [14,42]. Depending on current amplitude the thorax impedance is in the range of 20 Ω to 175 Ω and its variation is in the range of 100 mΩ to 2 Ω [14].

The current pump is one of the key components of ICG systems with a direct impact on their performance. The ICG systems need a high precision (minimum SNR = 95 dB in a 16 bit ICG system), wide bandwidth (tens or hundreds of kilo Hertz), and high output impedance (higher than hundreds of kΩ) current pump [14] in order to measure the ICG signal appropriately.

In this section, the relationships described in previous sections are used to design and implement an appropriate current pump for an ICG system. Standard HCP configuration (Fig. 1) can be a proper choice because in this configuration, the load is grounded and the output impedance and the compliance of the current pump are high. In comparison, the basic configuration has a significantly lower compliance, the bridge configuration floats the load, and the buffered feedback configuration has lower output impedance at high frequencies and higher output current error. Thus, a standard Howland circuit was designed to generate a 2 mA_{p-p} 50 kHz sinusoidal current. The peak of the derivative of this sine wave must be lower than the slew rate of the current pump and therefore, the minimum slew rate of HCP must be 314 μA/μs. To achieve the required gain (small β_{fb}, Eq. (3)) while maintaining output impedance (large R_{2b}, and tight matched and large resistors in the design, Eq. (13)) and the output compliance (small R_{2b}/R_{2a}, Eq. (4)) of the current pump, β_{fb} as considered 1/3 and R_{2a} and R_{2b}, 6 kΩ with 0.1% tolerance. Furthermore, to minimize the current error due to the offset voltage and input bias current of the op-amp, equal resistors for negative and positive feedback loops were considered, $R_2 = R_4 = 12$ kΩ (Eqs. (8) and (9)).

The output impedance of the current pump must be higher than 500 kΩ (assuming $R_{Load} = 500$ Ω, including the electrode-tissue impedance) if the error less than 0.1% in obtaining the tissue impedance (caused by finite output impedance of the current pump) and less than 0.2% in obtaining the tissue impedance variation is needed [3]. According to (13), to obtain 500 kΩ output impedance at 50 kHz, the open loop gain of the op-amp must be at least 55 dB. Note that in practice unintended stray capacitances degrade the output impedance, and therefore an op-amp with much greater open loop gain must be used to achieve the desired output impedance. Here, to achieve this, AD818, a low cost, high speed, dual supply operational amplifier with 70 dB open loop gain at 50 kHz was adopted for the desired HCP. For this, Eq. (13) gives 1.13 MΩ output impedance that is more than twice as much as what is required.

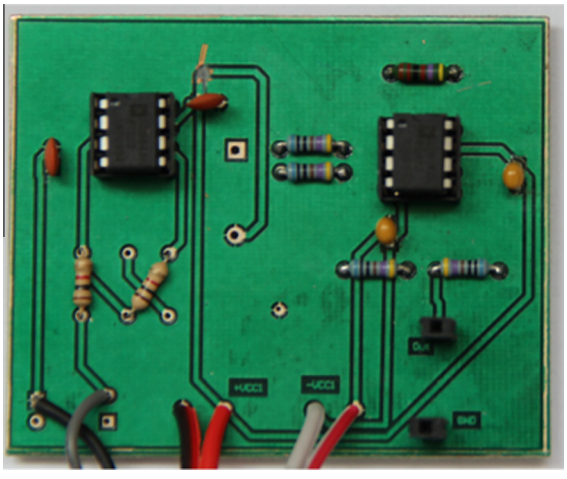

Fig. 7. The implemented Howland circuit using AD818 Op-Amp.

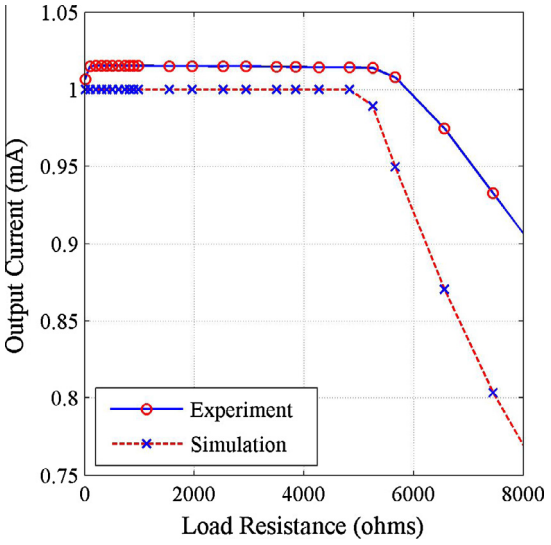

Fig. 8. Simulation and experimental results of the designed HCP's output current for different load values.

The slew rate of AD818 is equal to 500 V/μS. Assuming $R_{Load(max)} = 5.3$ KΩ (Eq. (4)), the slew rate of HCP will be 35.84 mA/μs (Eq. (16)), that is much larger than what is required. The supply voltage of the circuit was set to ±15 V. For an output current amplitude of 2 mAp-p, a sine wave voltage of 6 Vp-p was fed to negative input of HCP, and the positive input of HCP was grounded. In this way, the transfer function of the circuit becomes simpler (Eq. (15)) and the compliance will be 5.3 V (Eq. (4)).

In order to evaluate the practical performance of the designed HCP, the circuit was carefully constructed on a

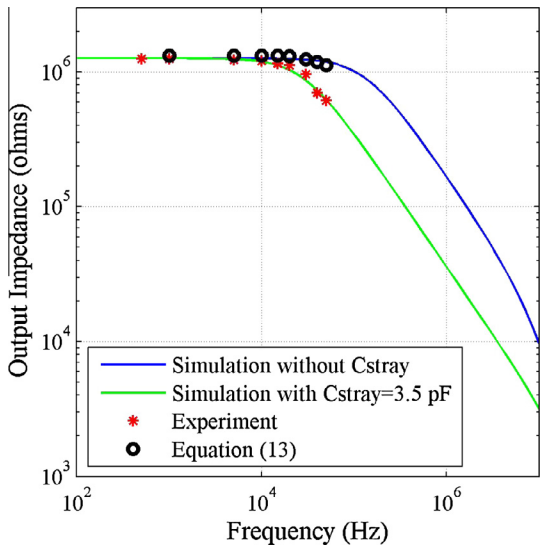

Fig. 9. Comparison of the output impedance of HCP measured in practice (stars), in simulation without stray capacitance (dash line), in simulation with 3.5 pF stray capacitance (solid line), and in theory (circles) without considering the stray capacitances.

two-layer printed circuit board. Symmetrical layout was used to achieve excellent matching (Fig. 7).

The sine wave was generated by AD9833, a direct digital synthesizer IC, which allows the precise adjustment of the desired waveform. The waveform was then amplified by an inverting amplifier using AD844. The output impedance of the amplifier was 0.2 Ω at 50 kHz.

The designed current pump was evaluated using a GW-INSTEK GDS-2304A digital storage oscilloscope (with the probe on 10X mode). Fig. 8 shows the measured output current for different load values from simulations and experiments. The simulation and experiment results are close (about 2% error) when the current pump is not saturated. The current amplitude is almost constant with the load until it reaches 5.4 KΩ. This value is close to the predicted value of 5.3 KΩ by Eq. (4) (relative error of 1.8%) and 5 KΩ from the simulations. The output was stable for different loads tested within the compliance of the current pump.

Measuring the high output impedance of HCP is challenging and requires very precise instrumentation [30]. Here, an ESCORT digital multimeter (model 3136A) was used to measure the current amplitude and the load resistance for which the output current is half of the value for no load (sort circuit output) was obtained, which is equal to the absolute value of output impedance of HCP. However, the AC current measurement bandwidth of this multimeter was 30 Hz–20 kHz. Therefore, at frequencies higher than 20 kHz, the drop technique was implemented using the GDS-2304A digital storage oscilloscope. Fig. 9 shows the measured output impedance in practice (stars) compared to the curve from simulation (dash line). The difference is mainly due to the stray capacitances at the output of HCP, and the input capacitance of the measurement probe. The solid curve demonstrates the output impedance from simulations when a capacitance of 3.5 pF was considered at the output of HCP, which is in good agreement with the measurements. About 1.7 pF of this capacitance can be considered as the measuring probe, while the rest can be due to the tracks on the board.

According to Eq. (15), considering the 100 MHz unity gain bandwidth of AD818 (for V_s = ±15 V), the bandwidth of the designed HCP should be 33 MHz (small signal bandwidth). The bandwidth obtained from the simulations confirms this value. However, the slew rate of the pump limits the maximum undistorted output frequency to 9.5 MHz considering the minimum Slew Rate of the op-amp which is 450 V/μs. The full power bandwidth of the pump was obtained 8.7 MHz in simulations and 9 MHz in practice.

The results of these experiments were close to the values predicted from theoretical equations and simulations. This confirms the validity of the derived equations, and emphasizes their importance and applicability for designing optimal HCP circuits.

Table 2 compares the performance characteristics of the designed HCP circuit with those in previous studies. All the circuits were implemented in TINA software, and the simulation results were provided. In order to have comparable results, simulation of the HCP design in this paper was repeated with 0.01% tolerance resistors. The results demonstrate that in this design, in addition to a very good

Table 2
Comparison of the performance characteristics of the HCP circuits designed in several studies based on simulations performed in TINA software.

Study	Design Parameters								R_{out} (MΩ)	I_{out} (mA)	Compliance (V) (Maximum Load (kΩ))	SNR[b] (dB)	Phase Margin (degree)
	β_{1b}	R_{2b}/R_{2a}	R_{2b} (kΩ)	R.Tole (%)	$A_{OL}(j\omega_{op})$ (dB)	f_{op} (kHz)	Vs						
Liu et al.[a] [31]	1/2	1	1	0.01	74	50	±5		1.68	2	2.2 (1.1)	84	×
Tucker et al. [30]	1/2	1	1	0.01	94.27	50	±5		3.24	1	2.1 (2.1)	108.6	63
Chen et al.[a] [32]	1/2	1	200	0	17.54	200	±5		0.49	0.005	0.5 (100)	×	×
Rafiei-Naeini et al. [41]	1/2	1	1	0.01	82.88	10	±12		2.16	1.4	6.77 (5)	109.3	×
This study	1/3	1	6	0.01	70	50	±15		3.26	1	5.17 (5.2)	99.7	72

[a] In references that more than one topology have been studied, only the results from standard HCP is presented.
[b] To make the SNR values comparable between designs, all the values were obtained by simulating the circuits at f_{op} = 50 kHz and R_L = 50 Ω.

phase margin, competitive output impedance, SNR and compliance were achieved despite using an op-amp with relatively moderate specifications. The design parameters in many of the previous studies is simply selected as equal R_{2a} and R_{2b} values and feedback ratio close to 0.5. However, significantly higher performance can be achieved by previous designs if these parameters are carefully adjusted, and the equations provided in this study can help to achieve this. For example, if the parameters used in this design were used in Tucker et al. [30] an output impedance as high as 12.82 MΩ with a phase margin of 64.2 degrees could be achieved (note that these values are simulation results without considering the parasitic impedances which are present in practice).

6. Discussion

In this study, the performance characteristics of different HCP configurations were theoretically studied, and it was shown that the important specifications of the pumps can be stated as functions of three major independent parameters: (1) the feedback ratio, β_{fb}, (2) the value of R_{2b}, and (3) the scale of the resistors used in positive and negative feedback paths. These parameters generally have not been considered in the design of HCP in previous published studies, while including them can significantly improve the performance of the designed pump for a specifically considered application.

Generally, in the design process, adopting a smaller R_{2b} improves the compliance, CMRR and slew rate, but degrades the output resistance and increases the static output error resulting from input offset voltage and bias current of the amplifier. Larger feedback ratio, β_{fb}, improves the output resistance, frequency bandwidth and the static output error of the HCP, while it increases the noise. The use of larger resistors also improves the input and output resistance and compliance at the expense of the increased noise. Therefore, a general guideline for the design of HCP is to use resistors as large as the noise level allows, with the feedback ratio close to one. Using large R_{2b} is necessary to ensure large output impedance, while the R_{2b} to R_{2a} ratio should be small. R_{2b} should be small also in comparison to the load impedance to achieve a high compliance. If the input is single (not differential), it is good to be applied to the negative input of the HCP because of its simpler transfer function toward the output.

The performance of the "basic" (or "simplified") HCP is generally lower than that in the standard configuration. The gain, compliance and CMRR are minimized and the static output errors are large in basic HCP. The bridge configuration has the advantage of twice as much compliance, as well as improved slew rate and output impedance, at the expense of an extra amplifier, and the load being float. HCP with buffered feedback path, in general, provides superior performance in comparison to the standard HCP. It usually exhibits improved compliance, output resistance, and CMRR.

None of the previous studies have considered the possible effect of CMRR on the output current systematic error. Slew rate may also affect the output signal. In many previous studies, the requirements for the op-amp used in the circuit have been neglected. Some authors [22,32] have concluded that output impedances larger than 1 MΩ cannot be achieved by HCP at the operation frequency, while some others have reported output impedances that seem impossible based on the equations derived in this study [31,41].

The output impedance of the HCP has an inverse relationship with the resistors tolerance. Therefore, in discrete implementation of the circuit, the use of trimmed resistor arrays is recommended. Another idea is to use "difference" amplifiers to benefit from their integrated trimmed resistors. The only disadvantage here is that the design would be restricted to the limited variation of available difference amplifiers. In the same manner, three op-amp instrumentation amplifiers, designed based on a difference amplifier, can be used with the benefit of high input impedance, and an extra resistor for adjusting the gain of the resulted HCP.

Stray capacitances degrade the overall output impedance at high frequencies by shunting current away from the load. A careful circuit implementation, including the use of only SMD components, short connections, avoiding parallel tracks, and isolating current-delivering traces from ground, can significantly reduce the effect of the stray capacitances [43]. If switches must be used to multiplex a single current source among multiple electrodes, capacitance cancellation system can be used to reduce their effective stray capacitance. Moreover, the use of a driven shield around the delivering current cables helps reduce the stray capacitance [44].

Simulations performed in TINA confirmed the validity of the derived equations. The practical implementation of a current pump for the ICG system confirmed the applicability of these equations in practice, both in the design process and for the prediction of the characteristics of the finally implemented HCP. Comparison of the HCP, designed in this study with several others proposed in the literature, demonstrated that higher performances can be achieved by proper selection of design parameters using the equations provided in this study.

References

[1] D. Prutchi, M. Norris, Design and Development of Medical Electronic Instrumentation: A Practical Perspective of the Design, Construction, and Test of Medical Devices, John Wiley & Sons, 2005.
[2] H. Yunfei, Development of a Bioimpedance based human machine interface, master thesis, Prince of Songkla University, 2009.
[3] D. Swanson, J. Webster, Errors in four-electrode impedance plethysmography, Med. Biol. Eng. Compute. 21 (1983) 674–680.
[4] I.S. Kim, J.K. Song, Y.L. Zhang, T.H. Lee, T.H. Cho, Y.M. Song, D.K. Kim, S.J. Kim, S.J. Hwang, Biphasic electric current stimulates proliferation and induces VEGF production in osteoblasts, BBA-Mol Cell Res. 1763 (2006) 907–916.
[5] P. Pouliquen, J. Vogelstein, R. Etienne-Cummings, Practical considerations for the use of a Howland current source for neurostimulation, IEEE Biomedical Circuits and Systems Conference (BioCAS), 2008, pp. 33–36.
[6] M. Schuettler, M. Franke, T.B. Krueger, T. Stieglitz, A voltage-controlled current source with regulated electrode bias-voltage for safe neural stimulation, J. Neurosci. Meth. 171 (2008) 248–252.
[7] C.J. Poletto, C.L. Van Doren, A high voltage, constant current stimulator for electrocutaneous stimulation through small electrodes, IEEE Trans. Biomed. Eng. 46 (1999) 929–936.

[8] M. Ghovanloo, K. Najafi, A compact large voltage-compliance high output-impedance programmable current source for implantable microstimulators, IEEE Trans. Biomed. Eng. 52 (2005) 97–105.
[9] E. Akhadov, A. Speed, D.P. Ryan, L.E. Matzen, Integration of Electroencephalography and Transcranial Direct Current Stimulation (tDCS) with High-Speed Operation, Electrode Re-Use, Automated tDCS Electrode Configuration, and Multiple Independent tDCS Curent Sources, Google Patents, 2011.
[10] A.S. Ross, G. Saulnier, J. Newell, D. Isaacson, Current source design for electrical impedance tomography, Physiol. Meas. 24 (2003) 509.
[11] D. Zhao, High output-impedance current source for electrical impedance tomography, in: 4th International IEEE Conference on Biomedical Engineering and Informatics (BMEI), 2011, pp. 1106–1109.
[12] C.-Y. Chen, Y.-Y. Lu, W.-L. Huang, K.-S. Cheng, The simulation of current generator design for multi-frequency electrical impedance tomograph, in: 28th Annual International IEEE Conference of Engineering in Medicine and Biology Society (EMBS), 2006, pp. 6072–6075.
[13] L. Constantinou, I.F. Triantis, R. Bayford, A. Demosthenous, High-power CMOS current driver with accurate transconductance for electrical impedance tomography, IEEE Trans. Biomed. Circuits Syst. 8 (2014) 575–583.
[14] G. Cybulski, Ambulatory Impedance Cardiography, Springer, 2011.
[15] C.-Y. Chiang, W.-C. Hu, L.-Y. Shyu, Portable impedance cardiography system for real-time noninvasive cardiac output measurement, in: Proceedings of the 19th Annual International IEEE Conference of Engineering in Medicine and Biology Society (EMBS), 1997, pp. 2072–2073.
[16] H. Zhang, J.K. Li, Noninvasive monitoring of transient cardiac changes with impedance cardiography, Cardiovasc. Eng. 8 (2008) 225–231.
[17] Y. Mohamadou, T.I. Oh, H. Wi, H. Sohal, A. Farooq, E.J. Woo, A.L. McEwan, Performance evaluation of wideband bio-impedance spectroscopy using constant voltage source and constant current source, Meas. Sci. Technol. 23 (2012) 105703.
[18] B. Karki, H. Wi, A. McEwan, H. Kwon, Evaluation of a multi-electrode bioimpedance spectroscopy tensor probe to detect the anisotropic conductivity spectra of biological tissues, Meas. Sci. Technol. 25 (2014) 075702.
[19] C. Toumazou, F. Lidgey, C. Makris, Extending voltage-mode op amps to current-mode performance, IEEE Proc.-G 137 (1990) 116–130.
[20] C. Denyer, F. Lidgey, Q. Zhu, C. McLeod, High output impedance voltage controlled current source for bio-impedance instrumentation, Proceedings of the 15th Annual International IEEE Conference of Engineering in Medicine and Biology Society (EMBS), 1993, pp. 1026–1027.
[21] R. Bragos, J. Rosell, P. Riu, A wide-band AC-coupled current source for electrical impedance tomography, Physiol. Meas. 15 (1994) A91.
[22] P. Bertemes-Filho, B. Brown, A. Wilson, A comparison of modified Howland circuits as current generators with current mirror type circuits, Physiol. Meas. 21 (2000) 1.
[23] J.J. Ackmann, Complex bioelectric impedance measurement system for the frequency range from 5 Hz to 1 MHz, Ann. Biomed. Eng. 21 (1993) 135–146.
[24] F. Seoane, R. Bragós, K. Lindecrantz, Current source for multifrequency broadband electrical bioimpedance spectroscopy systems. A novel approach, in: 28th Annual International IEEE Conference of Engineering in Medicine and Biology Society (EMBS), 2006, pp. 5121–5125.
[25] F. Seoane, R. Macias, R. Bragós, K. Lindecrantz, Simple voltage-controlled current source for wideband electrical bioimpedance spectroscopy: circuit dependences and limitations, Meas. Sci. Technol. 22 (2011) 115801.
[26] H. Hong, M. Rahal, A. Demosthenous, R.H. Bayford, Comparison of a new integrated current source with the modified Howland circuit for EIT applications, Physiol. Meas. 30 (2009) 999.
[27] D. Bouchaala, O. Kanoun, N. Derbel, High accurate and wideband current excitation for bioimpedance health monitoring systems, Measurement (2015). August.
[28] D. Sheingold, Impedance & admittance transformations using operational ampliifers, The Lightning Empiricist 12 (1964) 4.
[29] K.R. Aroom, M.T. Harting, C.S. Cox, R.S. Radharkrishnan, C. Smith, B.S. Gill, Bioimpedance analysis: a guide to simple design and implementation, J. Surg. Res 153 (2009) 23–30.
[30] A.S. Tucker, R.M. Fox, R.J. Sadleir, Biocompatible, high precision, wideband, improved Howland current source with lead-lag compensation, IEEE Trans. Biomed. Circuits Syst. 7 (2013) 63–70.
[31] J. Liu, X. Qiao, M. Wang, W. Zhang, G. Li, L. Lin, The differential Howland current source with high signal to noise ratio for bioimpedance measurement system, Rev. Sci. Instrum. 85 (2014) 055111.
[32] D. Chen, X. Deng, W. Yang, Comparison of three current sources for single-electrode capacitance measurement, Rev. Sci. Instrum. 81 (2010) 034704.
[33] Y. Wang, N. Li, H. Yu, Z. Sun, H. Nie, H. Xu, Study on Wide-band Voltage Controlled Current Source for Electrical Impedance Tomography, in: 2nd International IEEE Conference on Intelligent System Design and Engineering Application (ISDEA) 2012, pp. 1499–1502.
[34] J. Steele, T. Green, Tame those versatile current-source circuits, Feedback 2 (1992) H5.
[35] P. Bertemes-Filho, A. Felipe, The effect of the random distribution of electronic components in the output characteristics of the Howland current source, Journal of Physics: Conference Series, IOP Publishing, 2013, p. 012019.
[36] G. Hammond, C. Speake, M. Stiff, Noise analysis of a Howland current source, Int. J. Electron. 95 (2008) 351–359.
[37] L. Xiaoke, D. Feng, F. Yan, Analysis of constant-current characteristics for current sources, in: 24th Chinese IEEE conference on Control and Decision Conference (CCDC) 2012, pp. 2607–2612.
[38] T. Qureshi, C. Chatwin, N. Huber, A. Zarafshani, B. Tunstall, W. Wang, Comparison of Howland and General Impedance Converter (GIC) circuit based current sources for bio-impedance measurements, Journal of Physics: Conference Series, IOP Publishing, 2010, p. 012167.
[39] W. Wang, M. Brien, D. Gu, J. Yang, A comprehensive study on current source circuits, 13th International Conference on Electrical Bioimpedance and the 8th Conference on Electrical Impedance Tomography, Springer, 2007, pp. 213–216.
[40] H. Zumbahlen, Linear circuit design handbook, Newnes (2011).
[41] M. Rafiei-Naeini, H. McCann, Low-noise current excitation sub-system for medical EIT, Physiol. Meas. 29 (2008) S173.
[42] L. Geddes, L. Baker, The specific resistance of biological material—a compendium of data for the biomedical engineer and physiologist, Med. Biol. Eng 5 (1967) 271–293.
[43] F. Seoane, R. Bragós, K. Lindecrantz, P. Riu, Current source design for electrical bioimpedance spectroscopy, Encyclopedia Healthcare Inform. Syst. (2008) 359–367.
[44] G.J. Saulnier, D. Holder (Eds.), EIT Instrumentation, in Electrical Impedance Tomography: Methods, History and Applications, Inst. Physics Publishing, London, U.K., 2005, pp. 67–104.